AN1495

Average Current Mode Control of LLC Resonant Converter

Author: *Meeravali Shaik and Ramesh Kankanala*
Microchip Technology Inc.

ABSTRACT

Average Current Mode Control (ACMC) of a Pulse Frequency Modulated (PFM) LLC Resonant Converter considerably improves the dynamic response of the converter relative to other techniques, such as Voltage Mode Control (VMC). ACMC also facilitates meeting current sharing requirements of parallel connected converters. A good control loop bandwidth is required to meet the dynamic response specifictions and can be achieved using the ACMC-PFM LLC resonant converter. The plant transfer functions of the converter are derived using the Extended Describing Function (EDF), and appropriate compensators for the current and voltage control loops are designed. Experimental results verifying the model and design are presented and compared with the MATLAB® model results.

INTRODUCTION

In resonant converters, the operating principle is based on the characteristic gain curve of the resonant tank, where a variation of the switching frequency will change the gain. This results in an effective regulation of output voltage or current in relation to the load and input voltage changes. In the LLC resonant converter, the resonant tank is a set of two inductive elements and one capacitor (LLC).

The LLC resonant converter has several advantages over other traditional topologies. A few of them are as follows:

- LLC resonant converter can operate in both Step-up and Step-Down modes
- LLC resonant converter accommodates a wide range of output to input voltage ratios, with a relatively small frequency modulation range
- Soft switching (Zero Voltage Switching (ZVS)/ Zero Current Switching (ZCS)) could be achieved over the entire operating range

The primary side of the ACMC-LLC resonant converter has a half-bridge configuration, and the secondary side of the transformer has a center-tapped full wave rectifier and capacitive filter (C_f). A simple capacitor filter is used instead of a standard LC filter, thereby reducing the cost, component count and converter dimensions. The Q_1 and Q_2 MOSFETs are driven in Complementary mode at 50% duty cycle (neglecting the dead time). The resonant tank in the primary side of the converter has three passive components: magnetizing inductance (L_m), resonant capacitor (C_s) and series resonant inductor (L_s).

Modeling of the converter and compensator design for the ACMC-LLC resonant converter has been performed similar to the VMC-LLC resonant converter. Refer to *AN1477, "Digital Compensator Design for LLC Resonant Converter"* (DS01477) for more information.

In order to develop the state-space model for the ACMC-LLC resonant converter, the linearized plant model equations are inherited from the equations derived in the document, *AN1477, "Digital Compensator Design for LLC Resonant Converter"*. This application note describes the mathematical modelling and digital compensator design for the ACMC-LLC resonant converter.

Figure 1 illustrates the ACMC-LLC resonant converter.

FIGURE 1: SCHEMATIC OF AVERAGE CURRENT MODE CONTROLLED LLC RESONANT CONVERTER

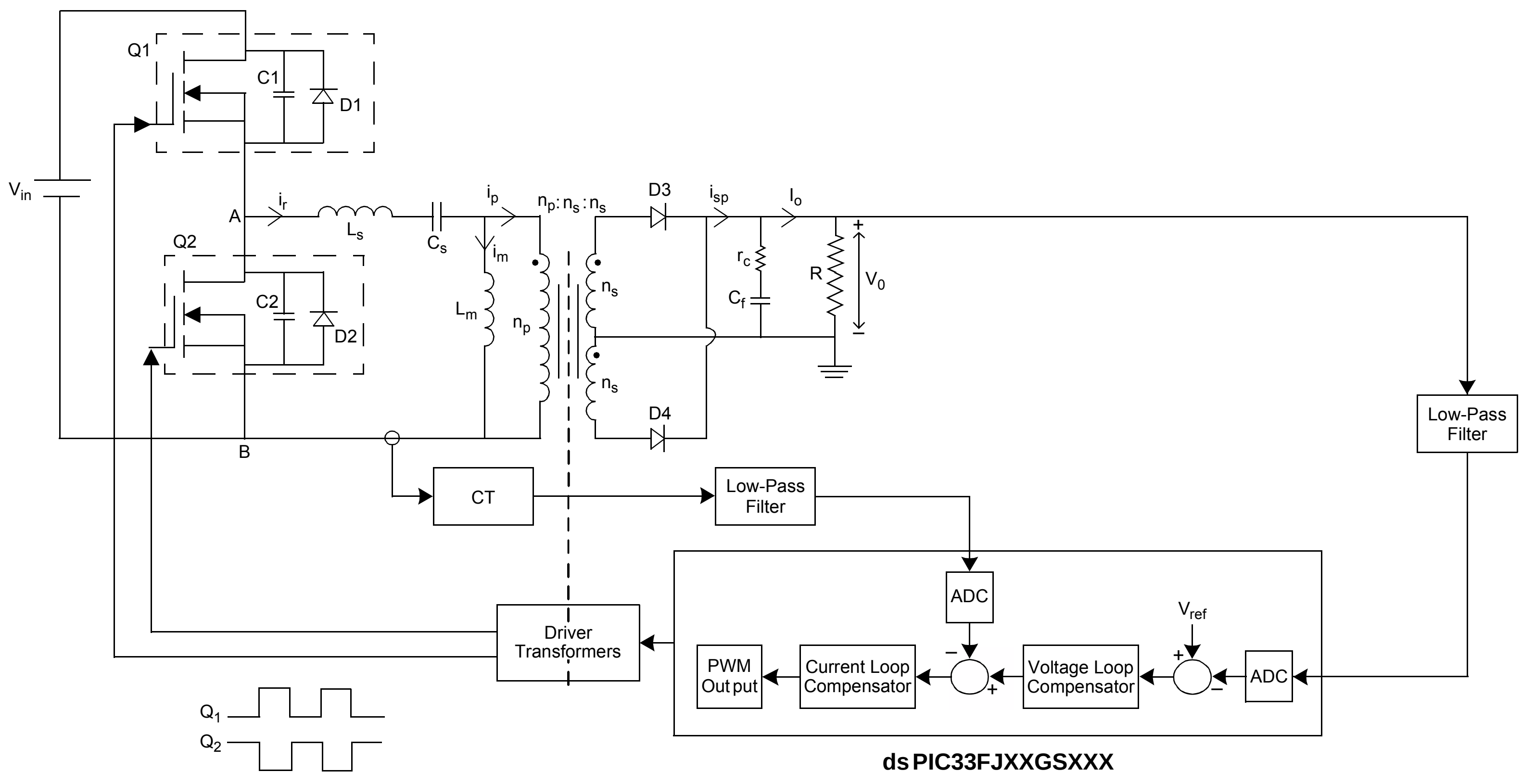

AVERAGE CURRENT MODE CONTROL VS. VOLTAGE MODE CONTROL

Current Mode Control (CMC) is a two-loop system, comprised of an inner current loop and an outer voltage loop (see Figure 1). The CMC method is widely used in Pulse-Width Modulation (PWM) converters and has the following advantages:

- Improved transient response: A CMC converter can be typically modeled as a first order system. Hence, it is easier to design a feedback network, and further, the overall transient response is improved.
- Improved disturbance rejection: The output of the constant current converter is nearly independent of variations in input voltage. This is achieved by a fast acting inner current loop which tightly controls the load current.
- Suitability for modular operation: When multiple converters are paralleled in an input-parallel/output-parallel combination, a common outer voltage feedback loop is sufficient for all paralleled converters. This configuration automatically enables equal or weighted load sharing through a common current reference for the individual inner current loops. The paralleled converters have the same control voltage, so there is equal load sharing.
- Self-protection against overload: The ACMC converter incorporates overload protection through the provision of limit checks to the current reference for the inner current loop.
- Transformer anti-saturation control: The current threshold control algorithm (inner current loop) automatically limits the maximum current through the transformer windings, thereby keeping the operating point of the transformer near the center of its B-H curve.

ACMC is implemented by sensing the resonant tank current (i_r in Figure 1) using a current sensing network (CT), which functions as a low-pass filter. This sensed current is fed to the current loop compensator. The reference to the inner current loop compensator is obtained from the output of the outer voltage loop compensator. The output of the current compensator defines the required operating frequency to be programmed to the PWM generator (PTPER register) for controlling the primary side MOSFETs of the half-bridge.

Plant Transfer Function

The plant transfer functions of the LLC resonant converter are derived using the EDFs. As mentioned in the Introduction, the modeling of the converter and compensator design for the ACMC-LLC resonant converter has been performed similar to the VMC-LLC resonant converter. Refer to Equation 23 in the application note, *AN1477, "Digital Compensator Design for LLC Resonant Converter"*, for deriving the large signal model of the LLC resonant converter.

The large signal model of the LLC resonant converter is provided in Equation 1.

EQUATION 1: LARGE SIGNAL MODEL OF LLC RESONANT CONVERTER

$$v_{es} = L_s\left(\frac{di_s}{dt} + \omega_s i_c\right) + r_s i_s + v_s + \frac{4n}{\pi}\frac{i_{ps}}{i_{pp}} v_{c_f}$$

$$v_{ec} = 0 = L_s\left(\frac{di_c}{dt} - \omega_s i_s\right) + r_s i_c + v_c + \frac{4n}{\pi}\frac{i_{pc}}{i_{pp}} v_{c_f}$$

$$i_s = C_s\left(\frac{dv_s}{dt} + \omega_s v_c\right)$$

$$i_c = C_s\left(\frac{dv_c}{dt} - \omega_s v_s\right)$$

$$L_m\left(\frac{di_{ms}}{dt} + \omega_s i_{mc}\right) = \frac{4n}{\pi}\frac{i_{ps}}{i_{pp}} v_{c_f} = v_{ps}$$

$$L_m\left(\frac{di_{mc}}{dt} - \omega_s i_{ms}\right) = \frac{4n}{\pi}\frac{i_{pc}}{i_{pp}} v_{c_f} = v_{pc}$$

$$\left(1 + \frac{r_c}{R}\right) C_f \frac{dv_{c_f}}{dt} + \frac{1}{R} v_{c_f} = \frac{2}{\pi} i_{sp}$$

$$v_0 = \frac{2}{\pi} r'_c\, i_{sp} + \left(\frac{r'_c}{r_c}\right) v_{c_f}$$

An equivalent circuit representation of the large signal model of the LLC resonant converter is illustrated in Figure 2.

FIGURE 2: LARGE SIGNAL MODEL OF LLC RESONANT CONVERTER

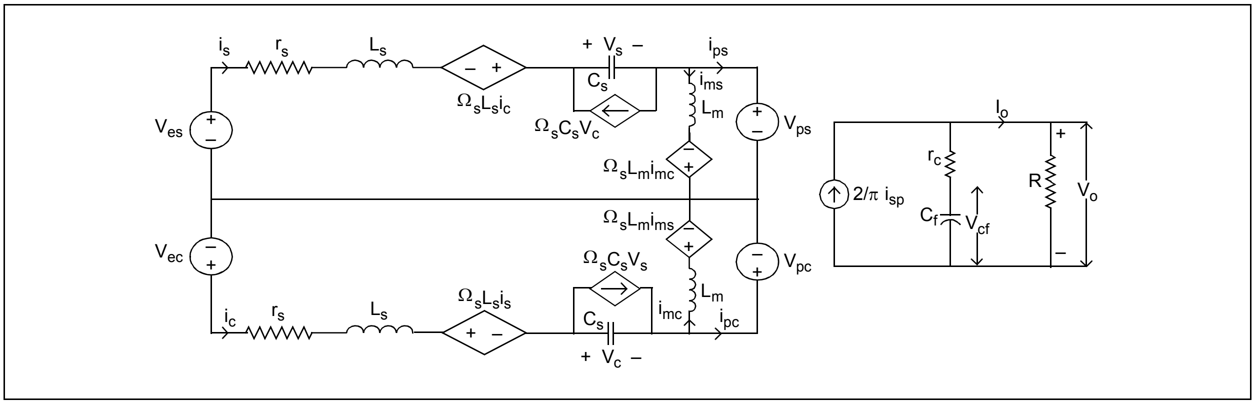

The following variables are used in Large Signal model:

- i_s and i_c: Sine and cosine components of the resonant inductor current
- i_{ms} and i_{mc}: Sine and cosine components of the magnetizing current
- V_s and V_c: Sine and cosine components of the resonant capacitor voltage
- V_{es} and V_{ec}: Sine and cosine components of the half-bridge output voltage
- V_{ps} and V_{pc}: Sine and cosine components of the transformer primary voltage
- i_{ps} and i_{pc}: Sine and cosine components of the transformer primary current
- i_p and r_s: Transformer primary current and DCR of the resonant Inductor
- i_{sp} and V_{cf}: Transformer secondary current and output filter capacitor voltage
- Ω_s and V_o: Steady-state switching frequency and output voltage
- C_f and r_c: Output filter capacitor and filter capacitor Equivalent Series Resistance (ESR)
- R and I_o: Load resistance and load current

The large signal model of the LLC resonant converter, provided in Equation 1, is perturbed and linearized about the chosen operating point to obtain small signal model equations. These equations are used to determine the plant transfer functions, such as output voltage-to-switching frequency ($G_{v\omega}(s)$) and inductor current-to-switching frequency ($G_{i\omega}(s)$) for ACMC.

The difference between the state-space models of VMC and ACMC is the presence of an additional output variable, which is the average inductor current (i_r) in the ACMC model.

The perturbation and linearization of the resonant inductor current is provided in Equation 2.

EQUATION 2: PERTURBATION AND LINEARIZATION OF RESONANT INDUCTOR CURRENT

$$i_r = \sqrt{i_s^2 + i_c^2}$$

Linearization of the Tank Current is:

$$\hat{i}_r = \frac{I_s}{\sqrt{I_s^2 + I_c^2}}\hat{i}_s + \frac{I_c}{\sqrt{I_s^2 + I_c^2}}\hat{i}_c = J_s\hat{i}_s + J_c\hat{i}_c$$

Where:

$$J_s = \frac{I_s}{\sqrt{I_s^2 + I_c^2}}$$

$$J_c = \frac{I_c}{\sqrt{I_s^2 + I_c^2}}$$

The linearized small signal model of the LLC resonant converter for ACMC is provided in Equation 3. Equation 3 incorporates the linearized resonant current, as derived in Equation 2.

EQUATION 3: LINEARIZED SMALL SIGNAL MODEL OF LLC RESONANT CONVERTER

$$\frac{d\hat{i}_s}{dt} = -\left(\frac{H_{ip}+r_s}{L_s}\right)\hat{i}_s - \left(\frac{\Omega_s L_s + H_{ic}}{L_s}\right)\hat{i}_c - \frac{1}{L_s}\hat{v}_s + \frac{H_{ip}}{L_s}\hat{i}_{ms} + \frac{H_{ic}}{L_s}\hat{i}_{mc} - \frac{H_{vcf}}{L_s}\hat{v}_{cf} + \frac{K_1}{L_s}\hat{v}_{in} + \frac{K_2}{L_s}\hat{d} - \frac{L_s\omega_0 I_c}{L_s}\hat{\omega}_{sn}$$

$$\frac{d\hat{i}_c}{dt} = \frac{(\Omega_s L_s - G_{ip})}{L_s}\hat{i}_s - \frac{(G_{ic}+r_s)}{L_s}\hat{i}_c - \frac{1}{L_s}\hat{v}_c + \frac{G_{ip}}{L_s}\hat{i}_{ms} + \frac{G_{ic}}{L_s}\hat{i}_{mc} - \frac{G_{vcf}}{L_s}\hat{v}c_f + \frac{L_s\omega_0 I_s}{L_s}\hat{\omega}_{sn}$$

$$\frac{d\hat{v}_s}{dt} = \frac{1}{C_s}\hat{i}_s - \frac{C_s\Omega_s}{C_s}\hat{v}_c - \frac{C_s\omega_0 V_c}{C_s}\hat{\omega}_{sn}$$

$$\frac{d\hat{v}_c}{dt} = \frac{1}{C_s}\hat{i}_c + \frac{C_s\Omega_s}{C_s}\hat{v}_s + \frac{C_s\omega_0 V_s}{C_s}\hat{\omega}_{sn}$$

$$\frac{d\hat{i}_{ms}}{dt} = \frac{H_{ip}}{L_m}\hat{i}_s + \frac{H_{ic}}{L_m}\hat{i}_c - \frac{H_{ip}}{L_m}\hat{i}_{ms} - \frac{(H_{ic}+L_m\Omega_s)}{L_m}\hat{i}_{mc} + \frac{H_{vcf}}{L_m}\hat{v}c_f - \frac{L_m I_{mc}\omega_0}{L_m}\hat{\omega}_{sn}$$

$$\frac{d\hat{i}_{mc}}{dt} = \frac{G_{ip}}{L_m}\hat{i}_s + \frac{G_{ic}}{L_m}\hat{i}_c - \frac{(G_{ip}-L_m\Omega_s)}{L_m}\hat{i}_{ms} - \frac{G_{ic}}{L_m}\hat{i}_{mc} + \frac{G_{vcf}}{L_m}\hat{v}c_f + \frac{L_m I_{ms}\omega_0}{L_m}\hat{\omega}_{sn}$$

$$\frac{d\hat{V}_{cf}}{dt} = \frac{K_{is}r'_c}{C_f r_c}\hat{i}_s + \frac{K_{ic}r'_c}{C_f r_c}\hat{i}_c - \frac{K_{is}r'_c}{C_f r_c}\hat{i}_{ms} - \frac{K_{ic}r'_c}{C_f r_c}\hat{i}_{mc} - \frac{r'_c}{RC_f r_c}\hat{v}_{cf}$$

The Output Equation is:

$$\hat{v}_0 = K_{is}r'_c\hat{i}_s + K_{ic}r'_c\hat{i}_c - K_{is}r'_c\hat{i}_{ms} - K_{ic}r'_c\hat{i}_{mc} + \left(\frac{r'_c}{r_c}\right)\hat{v}_{cf}$$

$$\hat{i}_r = J_s\hat{i}_s + J_c\hat{i}_c$$

Where:

$$H_{ip} = \frac{4nV_{c_f}}{\pi}\frac{I_{pc}^2}{I_{pp}^3}$$

$$H_{ic} = -\frac{4nV_{c_f}}{\pi}\frac{I_{ps}I_{pc}}{I_{pp}^3}$$

$$H_{vcf} = \frac{4n}{\pi}\frac{I_{ps}}{I_{pp}}$$

$$G_{ip} = -\frac{4nV_{c_f}}{\pi}\frac{I_{ps}I_{pc}}{I_{pp}^3}$$

$$G_{ic} = \frac{4nV_{c_f}}{\pi}\frac{I_{ps}^2}{I_{pp}^3}$$

$$G_{vcf} = \frac{4n}{\pi}\frac{I_{pc}}{I_{pp}}$$

$$K_1 = \frac{2}{\pi}\sin\left(\frac{\pi}{2}D\right)$$

$$K_2 = V_{in}\cos\left(\frac{\pi}{2}D\right)$$

$$K_{is} = \frac{2n}{\pi}\frac{I_{ps}}{\sqrt{I_{ps}^2 + I_{pc}^2}}$$

$$K_{ic} = \frac{2n}{\pi}\frac{I_{pc}}{\sqrt{I_{ps}^2 + I_{pc}^2}}$$

Formation of State-Space Model

State-space representation is a mathematical model of a physical system as a set of input, output and state variables, related by first order differential equations.

The state-space representation (known as time domain approach) provides a convenient and compact way to model and analyze systems with multiple inputs and outputs.

The linearized model obtained in Equation 3 is transformed into the state-space representation. The state-space model is used to obtain the transfer functions between output voltage and switching frequency ($G_{v\omega}(s)$), and between inductor current and switching frequency ($G_{i\omega}(s)$).

Equation 4 provides the state-space representation of the ACMC-LLC resonant converter.

EQUATION 4: STATE-SPACE MODEL OF LLC RESONANT CONVERTER

$$\frac{d\hat{x}}{dt} = A\hat{x} + B\hat{u}$$

$$\hat{y} = C\hat{x} + D\hat{u}$$

Where:

$$\hat{x} = \begin{bmatrix} \hat{i}_s & \hat{i}_c & \hat{v}_s & \hat{v}_c & \hat{i}_{ms} & \hat{i}_{mc} & \hat{v}_{c_f} \end{bmatrix}^T$$ States of the System

$$\hat{u} = \begin{bmatrix} \hat{f}_{sn} \ or \ \hat{\omega}_{sn} \end{bmatrix}$$ Control Inputs and All Other Disturbance Inputs are Ignored

$$\hat{y} = \begin{bmatrix} \hat{v}_o \\ \hat{i}_r \end{bmatrix}$$ Outputs

$$A = \begin{bmatrix} -\frac{H_{ip}+r_s}{L_s} & -\frac{(\Omega_s L_s + H_{ic})}{L_s} & -\frac{1}{L_s} & 0 & \frac{H_{ip}}{L_s} & \frac{H_{ic}}{L_s} & -\frac{H_{vcf}}{L_s} \\ \frac{\Omega_s L_s - G_{ip}}{L_s} & -\frac{G_{ic}+r_s}{L_s} & 0 & -\frac{1}{L_s} & \frac{G_{ip}}{L_s} & \frac{G_{ic}}{L_s} & -\frac{G_{vcf}}{L_s} \\ \frac{1}{C_s} & 0 & 0 & -\frac{C_s\Omega_s}{C_s} & 0 & 0 & 0 \\ 0 & \frac{1}{C_s} & \frac{C_s\Omega_s}{C_s} & 0 & 0 & 0 & 0 \\ \frac{H_{ip}}{L_m} & \frac{H_{ic}}{L_m} & 0 & 0 & -\frac{H_{ip}}{L_m} & -\frac{H_{ic}+L_m\Omega_s}{L_m} & \frac{H_{vcf}}{L_m} \\ \frac{G_{ip}}{L_m} & \frac{G_{ic}}{L_m} & 0 & 0 & -\frac{G_{ip}-L_m\Omega_s}{L_m} & -\frac{G_{ic}}{L_m} & \frac{G_{vcf}}{L_m} \\ \frac{K_{is}r'_c}{C_f r_c} & \frac{K_{ic}r'_c}{C_f r_c} & 0 & 0 & -\frac{K_{is}r'_c}{C_f r_c} & -\frac{K_{ic}r'_c}{C_f r_c} & -\frac{r'_c}{RC_f r_c} \end{bmatrix}$$

$$B = \begin{bmatrix} -\frac{L_s\omega_0 I_c}{L_s} & \frac{L_s\omega_0 I_s}{L_s} & -\frac{C_s\omega_0 V_c}{C_s} & \frac{C_s\omega_0 V_s}{C_s} & -\frac{L_m\omega_0 I_{mc}}{L_m} & \frac{L_m\omega_0 I_{ms}}{L_m} & 0 \end{bmatrix}$$

$$C = \begin{bmatrix} K_{is}r'_c & K_{ic}r'_c & 0 & 0 & -K_{is}r'_c & -K_{ic}r'_c & \frac{r'_c}{r_c} \\ J_s & J_c & 0 & 0 & 0 & 0 & 0 \end{bmatrix}$$

$$D = \begin{bmatrix} 0 \\ 0 \end{bmatrix}$$

From the state-space model in Equation 4, the control-to-output voltage transfer function ($G_{v\omega}(s)$) and the control-to-inductor current transfer function ($G_{i\omega}(s)$) are provided in Equation 5, where the control variable is the PWM switching frequency of an LLC resonant converter.

EQUATION 5: ($G_{i\omega}(s)$) AND ($G_{v\omega}(s)$) TRANSFER FUNCTIONS

$$\begin{bmatrix} \hat{v}_0/\hat{\omega}_{sn} \\ \hat{i}_r/\hat{\omega}_{sn} \end{bmatrix} = C(sI-A)^{-1}B + D = \begin{bmatrix} G_{v\omega}(s) \\ G_{i\omega}(s) \end{bmatrix}$$

Equation 5 is solved in order to obtain the $G_{v\omega}(s)$ and $G_{i\omega}(s)$ transfer functions.

HARDWARE DESIGN SPECIFICATIONS

Series resonant inductor (L_s) = 62 µH

Series resonant capacitance (C_s) = 9.4 nF

Magnetizing inductor (L_m) = 268 µH

Input voltage (V_{in}) = 400V (DC)

Output filter capacitance (C_f) = 2000 µF

Output power = 200W

Switching frequency (f_s) = 200 kHz

DC Resistance (DCR) of resonant inductor (r_s) = 15 mΩ

ESR of output capacitor (r_c) = 15 mΩ

Transformer turns ration (n) = 16.667

Equation 1 provides the MATLAB commands to obtain the $G_{v\omega}(s)$ and $G_{i\omega}(s)$ transfer functions.

EXAMPLE 1: MATLAB® COMMANDS

```
sys=ss(A,B,C,D);     % arranges the A,B,C,D
matrices into a state-space model
H=tf(sys);           % Plant transfer functions
```

PLANT TRANSFER FUNCTION

After solving Equation 5, using Example 1 with the hardware design specifications, $G_{i\omega}(s)$ and $G_{v\omega}(s)$ are provided in Equation 6 and Equation 7. In resonant converters, the poles and zeroes are the functions of the normalized switching frequency ($\omega_{sn} = \omega_s/\omega_0$). Where, ω_s = switching frequency and ω_0 = resonant frequency.

Equation 6 and Equation 7 are obtained after neglecting the poles and zeros above the switching frequency (ω_s).

EQUATION 6: INDUCTOR CURRENT-TO-SWITCHING FREQUENCY TRANSFER FUNCTION

$$G_{i\omega}(s) = \frac{1.2573 \times \left(\frac{s}{1174} + 1\right)}{\left(\frac{s^2}{(1.107 \times 10^6)^2} + \frac{2.76 \times 10^5 s}{1.107 \times 10^6} + 1\right)\left(\frac{s^2}{(2.99 \times 10^4)^2} + \frac{973.6s}{2.99 \times 10^4} + 1\right)}$$

The General Form of $G_{i\omega}(s)$:

$$G_{i\omega}(s) = \frac{G_{co} \times \left(1 + \frac{s}{\omega_{esr}}\right)}{\left(\frac{s^2}{\omega_{p1}^2} + \frac{s}{(Q_1 \cdot \omega_{p1})} + 1\right) \times \left(\frac{s^2}{\omega_{p2}^2} + \frac{s}{(Q_2 \cdot \omega_{p2})} + 1\right)}$$

EQUATION 7: OUTPUT VOLTAGE-TO-SWITCHING FREQUENCY TRANSFER FUNCTION

$$G_{v\omega}(s) = \frac{5.56 \times \left(\frac{s}{3.314 \times 10^4} + 1\right) \times \left(\frac{s}{8.262 \times 10^5} - 1\right)}{\left(\frac{s^2}{(1.107 \times 10^6)^2} + \frac{2.76 \times 10^5 s}{1.107 \times 10^6} + 1\right)\left(\frac{s^2}{(2.99 \times 10^4)^2} + \frac{973.6s}{2.99 \times 10^4} + 1\right)}$$

Digital Compensator Design for ACMC-LLC Resonant Converter

The ACMC-LLC resonant converter control system is comprised of two loops: an inner current loop and an outer voltage loop, as illustrated in Figure 3. The inner current loop directly controls the inductor current. The output of the inner current loop defines the frequency of the PWM module to drive the half-bridge MOSFETs. The outer voltage loop controls the output voltage by generating the current reference for the inner current loop. To ensure stable operation of the multi-loop converter, all the sequential loops in the circuit should be stable with a sufficient degree of stability.

The digital compensator is designed for the plant transfer functions, as obtained in Equation 6. For stable operation of a multi-loop control system, the inner current loop must be faster than the outer voltage loop.

In order to achieve a higher bandwidth for the inner current loop, and satisfy the gain margin and phase margin stability requirements, a digital 2-Pole 2-Zero (2P2Z) compensator has been chosen. A digital PI compensator has been chosen for the outer voltage loop.

The digital compensators have been derived using the design by emulation or digital redesign approach. In this approach, the compensator is designed in the continuous time domain and then converted to discrete time domain using the Bilinear or Tustin transformation.

FIGURE 3: CONTROL LOOP BLOCK DIAGRAM OF ACMC-LLC RESONANT CONVERTER

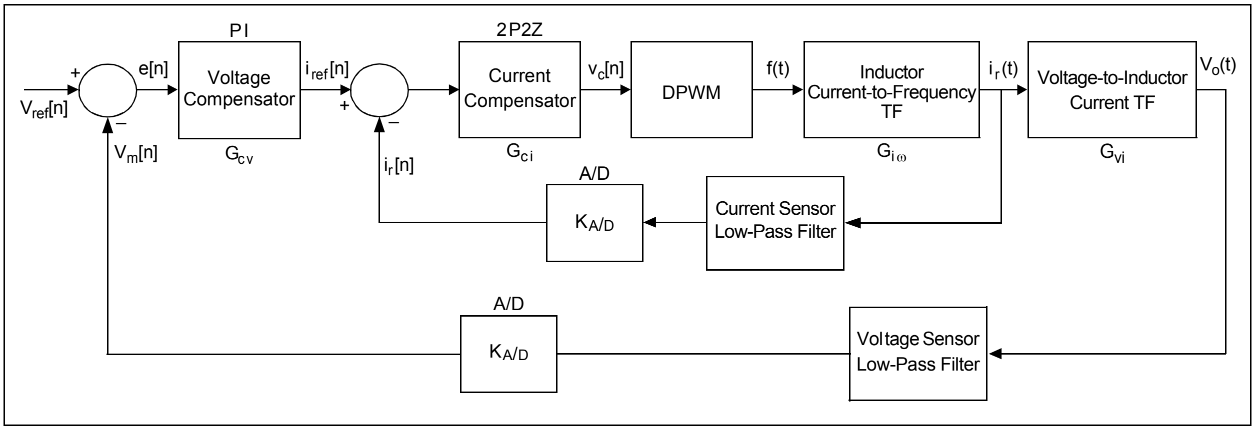

Inner Current Loop

The inner current loop compensator is designed to control the frequency to inductor current transfer function of the converter ($G_{i\omega}(s)$). The inner current loop ($V_c[n]$) directly controls the inductor current.

The output of the inner current loop defines the frequency of the PWM module output to drive the half-bridge MOSFETs. The frequency response of Equation 6 is illustrated in Figure 4.

FIGURE 4: FREQUENCY RESPONSE OF INDUCTOR CURRENT-TO-SWITCHING FREQUENCY TRANSFER FUNCTION

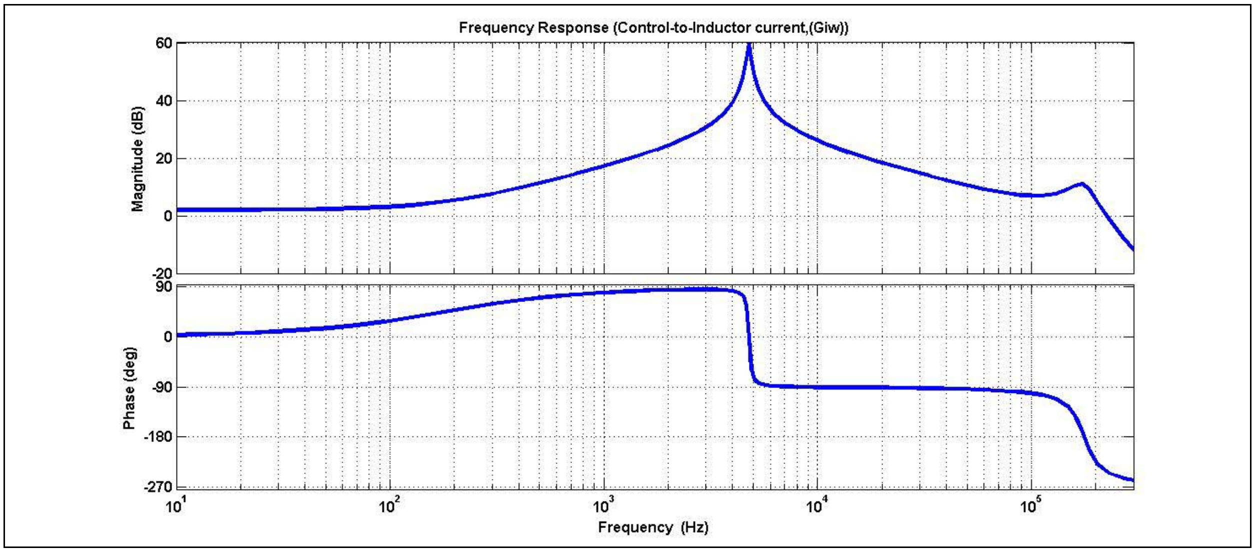

The control block diagram for the inner current loop, including the low-pass filter (G_{fc}), computation and digital delay (G_{delay}), digital 2-Pole 2-Zero (2P2Z) (G_{ci}) compensator and PWM (G_{PWM}) is illustrated in Figure 5.

FIGURE 5: CONTROL BLOCK DIAGRAM OF INNER CURRENT LOOP

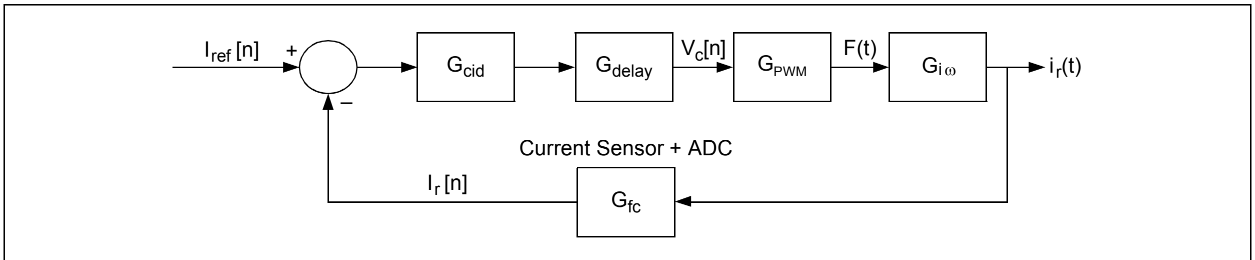

A first order low-pass filter (G_{fc}) is provided to filter the resonant tank current using a current transformer or any other current sensing network. The low-pass filter transfer function is provided in Equation 8.

EQUATION 8: CURRENT SENSOR NETWORK LOW-PASS FILTER TRANSFER FUNCTION

$$G_{fc}(s) = \frac{1}{(R_{fc}C_{fc}s + 1)}$$

Where:

$R_{fc} = 10\Omega$

$C_{fc} = 10\ \mu F$

The inductor current to switching frequency plant transfer function, provided in Equation 6, consists of a zero due to the ESR (ω_{esr}) of the output filter capacitor and a pair of dominant complex poles. To compensate the increased gain at high frequency, and thereby increasing the ripple effect due to ESR zero, a pole (ω_p) is included in the compensator. In order to minimize the steady-state error, an integrator (K_{ci}) is added to the compensator.

To compensate for reduction in system damping, and hence, increased overshoots, increased settling time due to the effect of the complex dominant poles, two zeros ($s+\alpha+j\beta$) and ($s+\alpha-j\beta$) are added.

Effectively, the inner current loop control system will have a 2-Pole 2-Zero (2P2Z) compensator in the continuous domain, as provided in Equation 9.

EQUATION 9: 2P2Z COMPENSATOR ($G_{ci}(s)$) IN CONTINUOUS TIME DOMAIN

$$G_{ci}(s) = \frac{K_{ci} \times \left(\frac{s^2}{\omega_z^2} + \frac{s}{Q_c \times \omega_z} + 1\right)}{s \times \left(\frac{s}{\omega_p} + 1\right)}$$

$$= \frac{\left(\frac{K_{ci}}{\omega_z^2}\right) \times (s + \alpha + j\beta) \times (s + a - j\beta)}{s \times \left(\frac{s}{\omega_p} + 1\right)}$$

The compensator pole, ω_p ($2\pi f_p$), is placed at ω_{esr} (1.17k radians/second) to cancel the ESR zero. A pair of complex zeros is included in the compensator transfer function at locations, $s_1 = -487+j29.9k\ (-\alpha+j\beta)$ and $s_2 = -487-j29.9k\ (-\alpha-j\beta)$, having a corner frequency (ω_z). ω_z is chosen slightly below or equal to the corner frequency of the dominant resonant poles (ω_{p1}) (29.9k radians/second) to provide the necessary phase lead. K_{ci} represents the integrator gain of the compensator and is adjusted to achieve the desired crossover frequency of the converter. In this analysis, computation and digital delay, and PWM gain, are assumed to be unity.

The desired crossover frequency is f_{ci} in Hz and $\omega_{ci} = j2\pi f_{ci}$ in radians/second. At crossover frequency, the loop gain of the system should be 0 dB or one in linear scale. The inner current loop compensator gain calculation is provided in Equation 10.

EQUATION 10: INNER CURRENT LOOP COMPENSATOR GAIN CALCULATION

$$G_{i\omega}(s)\big|_{s = \omega_{ci}} \times G_{ci}(s)\big|_{s = \omega_{ci}} = 1$$

The Required Gain of the Compensator is:

$$K_{ci} = \frac{1}{G_{i\omega}(s)\big|_{s = \omega_{ci}} \times G_{ci}(s)\big|_{s = \omega_{ci}}}$$

It is to be noted that in Equation 10, the magnitude of $G_{ci}(s)$ is calculated by excluding K_{ci}. The resulting compensator for achieving a crossover frequency of 5000 Hz is provided in Equation 11.

EQUATION 11: INNER CURRENT LOOP COMPENSATOR TRANSFER FUNCTION ($G_{ci}(s)$)

$$G_{ci}(s) = \frac{0.032753 \times (s^2 + 973.6s + (2.99 \times 10^4)^2)}{s \times (s + 1174)}$$

The inner current loop gain is the product of gains around the forward path and feedback path of the loop, as provided in Equation 12. Equation 12 shows how the addition of a feedback loop modifies the transfer functions and performance of the inner current loop.

EQUATION 12: INNER CURRENT LOOP GAIN

$$Inner\ Current\ Loop\ Gain = G_{fc}(s) \times G_{ci}(s) \times G_{delay}(s) \times G_{PWM}(s) \times G_{i\omega}(s)$$

Where:

$G_{delay}(s)$ = Transfer Functions of Transportation Delay

$G_{ci}(s)$ = Transfer Function of the Inner Current Loop Compensator

$G_{fc}(s)$ = Current Sensor Network Low-Pass Filter

$G_{PWM}(s)$ = PWM Module Gain

Frequency response of the inner current loop gain in Equation 12 is illustrated in Figure 6, and it is observed that the crossover frequency is ~5 kHz.

FIGURE 6: FREQUENCY RESPONSE PLOT OF LOOP GAIN (INNER CURRENT LOOP)

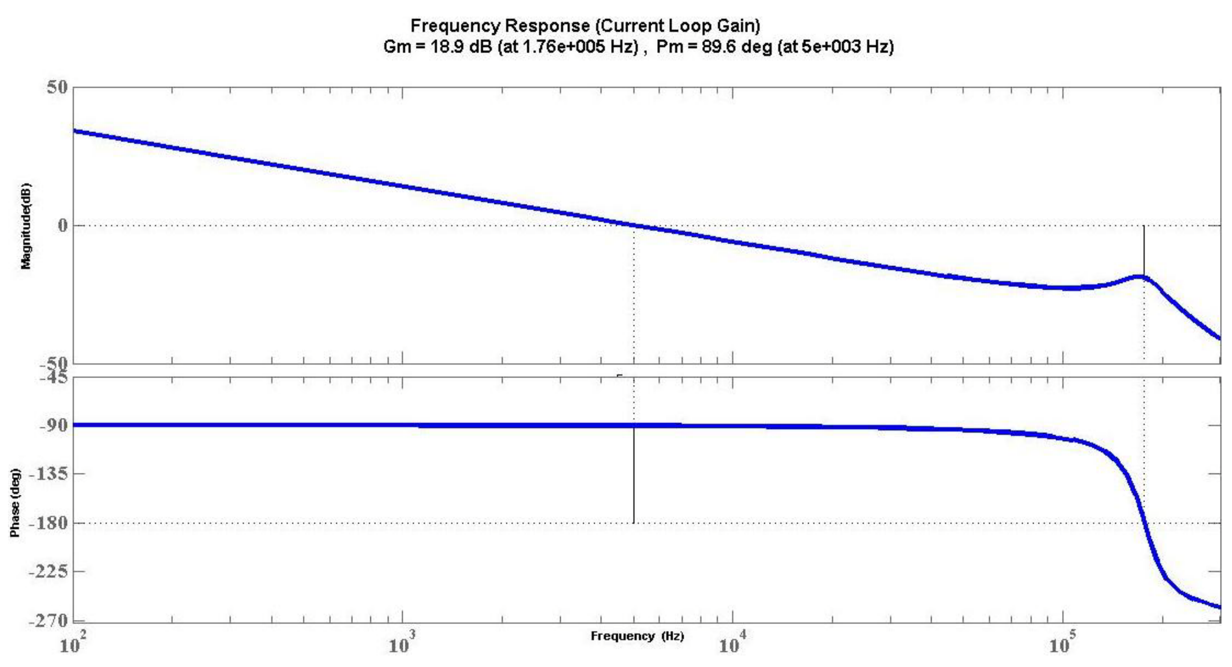

The continuous domain 2-Pole 2-Zero (2P2Z) compensator in Equation 11 is converted to z-domain using the Tustin or Bilinear transformation, where $s = 2/T_s\ [(z-1)/(z+1)]$ with a sampling frequency of 50 kHz. The z-domain compensator transfer function ($G_{cid}(z)$) is provided in Equation 13.

EQUATION 13: INNER CURRENT LOOP COMPENSATOR TRANSFER FUNCTION IN DISCRETE DOMAIN ($G_{cid}(z)$)

$$G_{cid}(z) = \frac{0.03558z^2 - 0.05895z + 0.03495}{z^2 - 1.976z + 0.9767}$$

Outer Voltage Loop

The outer voltage loop controls the output voltage (V_o) by generating a current reference ($I_{ref}(n)$) for the inner current loop. To ensure stable operation of the multi-loop converter, all the sequential loops (inner current loop in this application) in the circuit should be stable with sufficient stability. The outer voltage loop control system block diagram is illustrated in Figure 7.

FIGURE 7: CONTROL SYSTEM BLOCK DIAGRAM OF OUTER VOLTAGE LOOP

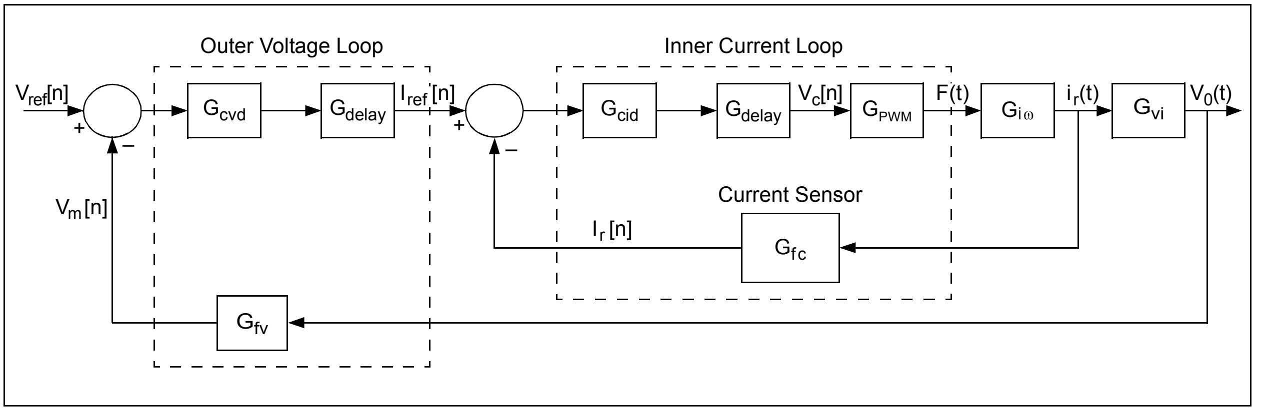

From Figure 7, it is clear that the closed loop transfer function of inner current loop is necessary to obtain the frequency response of the outer voltage loop. The closed loop transfer function of inner current loop (G_{iCL}) is provided in Equation 14 and this includes the transfer function of the forward path and feedback path.

EQUATION 14: CLOSED LOOP TRANSFER FUNCTION OF INNER CURRENT LOOP ($G_{iCL}(s)$)

$$G_{iCL}(s) = \frac{i_r(s)}{i_{ref}(s)}$$

$$= \frac{G_{ci}(s) \times G_{delay}(s) \times G_{PWM}(s) \times G_{i\omega}(s)}{1 + G_{fc}(s) \times G_{ci}(s) \times G_{delay}(s) \times G_{PWM}(s) \times G_{i\omega}(s)}$$

For the outer voltage loop, the plant transfer function will be the inductor current-to-output voltage transfer function ($G_{vi}(s)$), as provided in Equation 15.

EQUATION 15: INDUCTOR CURRENT-TO-OUTPUT VOLTAGE TRANSFER FUNCTION ($G_{vi}(s)$)

$$G_{vi}(s) = \frac{G_{v\omega}(s)}{G_{i\omega}(s)}$$

$$= \frac{1.9067 \times 10^{-7} \times (s - 8.26 \times 10^5) \times (s + 3.314 \times 10^7)}{(s + 1174)}$$

A first order low-pass filter has been used for filtering high-frequency noise from the output voltage measurement. This filter transfer function is provided in Equation 16.

EQUATION 16: LOW-PASS FILTER TRANSFER FUNCTION ($G_{fv}(s)$)

$$G_{fv}(s) = \frac{1}{(R_{fv}C_{fv}s + 1)}$$

Where:

$R_{fv} = 1153\Omega$

$C_{fv} = 2200\ pF$

The outer voltage loop gain is the product of gains around the forward path and feedback path of the loop are provided in Equation 17, and this includes the closed loop transfer function of the inner current loop.

EQUATION 17: OPEN-LOOP GAIN OF OUTER VOLTAGE LOOP ($G_{vl}(s)$)

Open-Loop Gain of the Outer Voltage Loop:

$$G_{vl}(s) = G_{delay}(s) \times G_{iCL}(s) \times G_{vi}(s)$$

Open-loop gain of the outer voltage loop frequency response is illustrated in Figure 8.

FIGURE 8: FREQUENCY RESPONSE OF OPEN-LOOP GAIN OF OUTER VOLTAGE LOOP

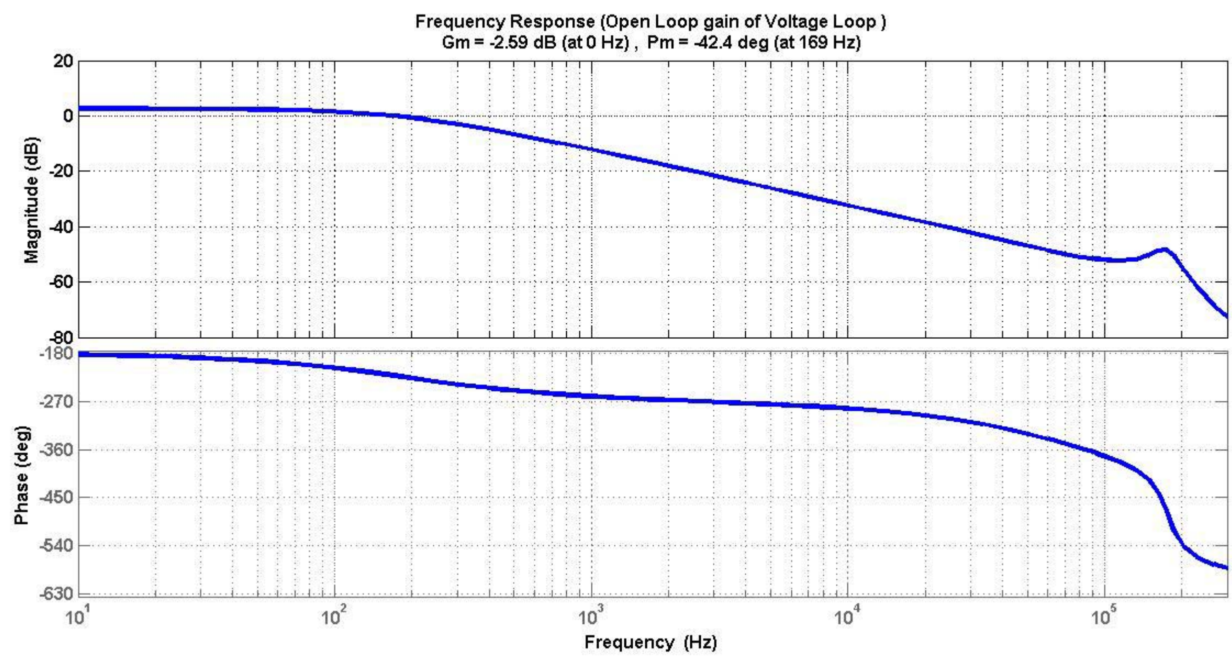

The voltage PI compensator theoretically produces infinite gain at DC. As a result, a zero steady-state voltage error can be achieved. The proportional gain is tuned to achieve the desired crossover frequency.

The current compensator nullifies the effect of the complex dominant poles (ω_{p1}), thereby simplifying the design of the outer voltage loop compensator (G_{cv}).

The general form of a PI compensator in continuous domain is given in Equation 18.

EQUATION 18: OUTER VOLTAGE LOOP PI COMPENSATOR ($G_{cv}(s)$) TRANSFER FUNCTION

$$G_{cv}(s) = K_p + \frac{K_i}{s} = \frac{K_{cv}(s + \omega_v)}{s}$$

Where:

K_p = Proportional Gain

K_i = Integral Gain

K_{cv} = Gain of PI Compensator

ω_v = Magnitude of PI Compensator Zero in Radians/Second

The desired crossover frequency is f_{cv} in Hz and $\omega_{cv} = j2\pi f_{cv}$ in radians/second. At crossover frequency, the loop gain of the system should be 0 dB or one in linear scale, as provided in Equation 19. The magnitude of $G_{cv}(s)$ is calculated by excluding K_{cv}.

EQUATION 19: COMPENSATOR GAIN CALCULATION

$$G_{vl}(s)|_{s = \omega_{cv}} \times G_{cv}(s)|_{s = \omega_{cv}} = 1$$

The Required Gain of the Compensator is:

$$K_{cv} = \frac{1}{G_{vl}(s)|_{s = \omega_{ci}} \times G_{cv}(s)|_{s = \omega_{cv}}}$$

The PI compensator zero (ω_v) is placed at 25000 radians/second to obtain the required phase at a crossover frequency of 3000 Hz, as provided in Equation 20.

EQUATION 20: COMPENSATOR TRANSFER FUNCTION ($G_{cv}(s)$)

$$G_{cv}(s) = \frac{7.3(s + 25000)}{s} = \frac{7.3s + 1.82 \times 10^5}{s}$$

The compensated converter loop gain ($G_{vs}(s)$) transfer function is provided in Equation 21.

EQUATION 21: CONVERTER LOOP GAIN ($G_{vs}(s)$)

Converter Loop Gain:

$$G_{vs}(s) = G_{fv}(s) \times G_{cv}(s) \times G_{delay}(s) \times G_{iCL}(s) \times G_{vi}(s)$$

The frequency response is illustrated in Figure 9.

FIGURE 9: CONVERTER LOOP GAIN

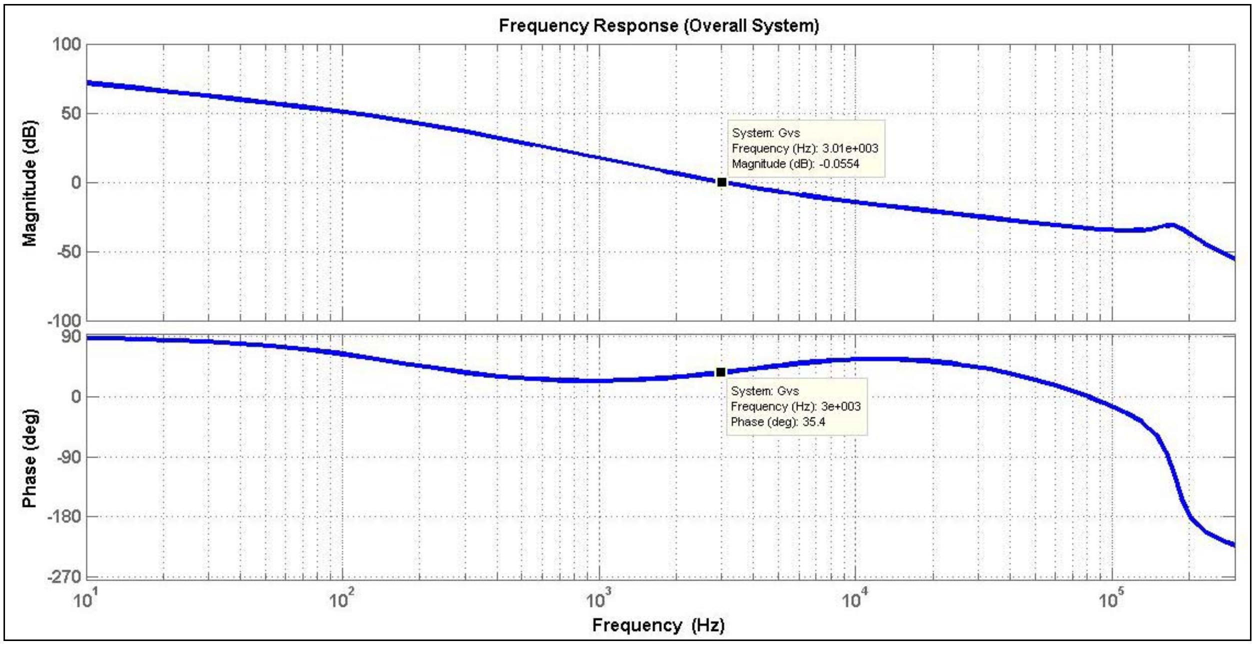

Simulation results in Figure 9 indicate that the crossover frequency of the converter is at 3 kHz.

Figure 10 illustrates the measured loop gain obtained from the network analyzer. The measured crossover frequency of the converter is very close to 3 kHz, thereby confirming the model prediction.

FIGURE 10: MEASURED LOOP GAIN OF THE CONVERTER

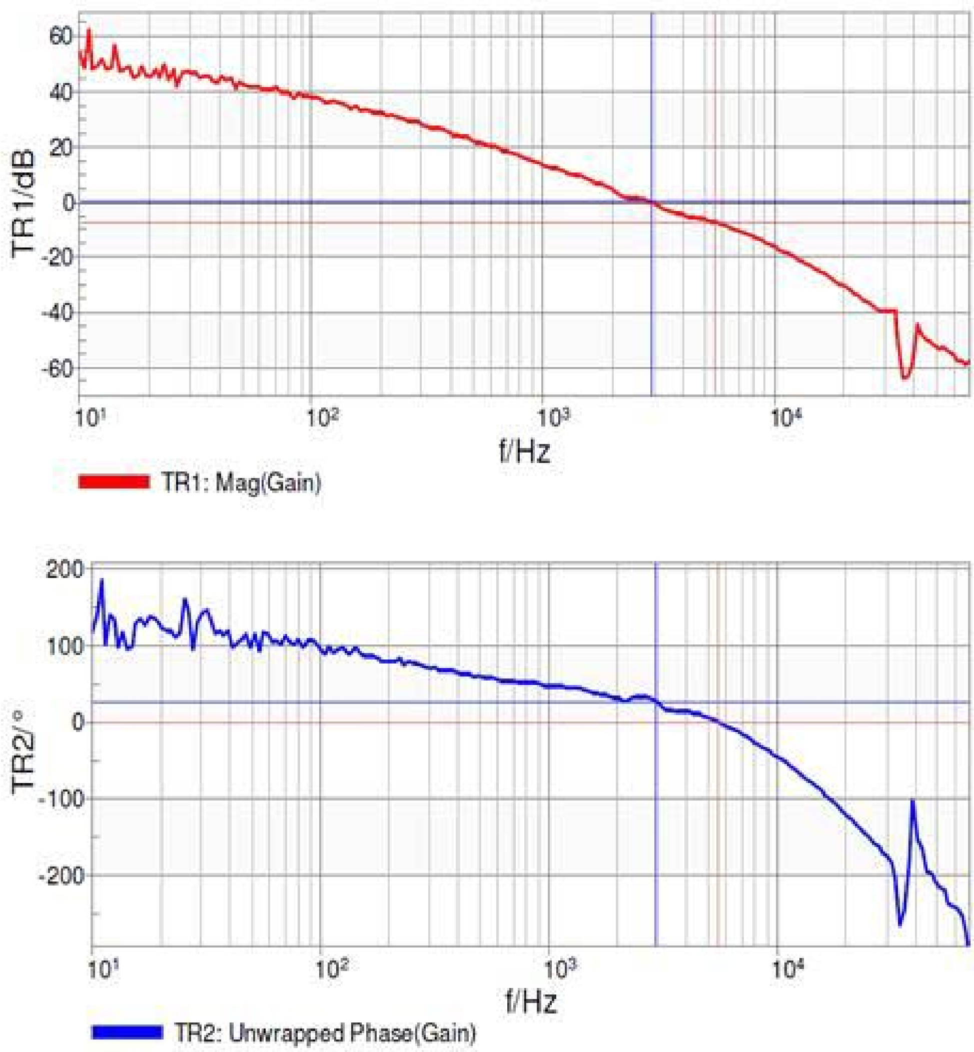

Cursor	Frequency	Trace 1	Trace 2
Red Cursor 1 :	5.496 kHz	-7.178 dB	130.175 m°
Blue Cursor 2 :	2.939 kHz	0.083 dB	26.628 °
Delta :	-2.556 kHz	7.261 dB	26.498 °

CONCLUSION

Average Current Mode Controlled (ACMC) Pulse Frequency Modulated (PFM) LLC resonant converter plant transfer function is derived by employing Extended Describing Functions (EDF). The ACMC-LLC resonant converter has superior noise immunity, and provides good dynamic response and current sharing requirements of parallel connected converters. A multi-loop digital compensator is designed to meet the specifications of phase margin, gain margin and bandwidth for the converter. The hardware results or waveforms are in conformity to the developed analytical model and also meet the target specifications.

REFERENCES

- *AN1477, "Digital Compensator Design for LLC Resonant Converter"* (DS01477)
- *"Small-Signal Modeling of Series and Parallel Resonant Converters"*, by Yang E.X; Lee F.C; Jovanovich M.M, Applied Power Electronics Conference and Exposition, 1992. APEC' 92. Conference Proceedings 1992, Seventh Annual,1992, Page(s): 785-792
- *"Approximate Small-Signal Analysis of the Series and the Parallel Resonant Converters"*, by Voperian V, Power Electronics, IEEE Transactions on, Vol. 4, Issue 1, January 1989, Page(s): 15-24
- *AN1336, "DC/DC LLC Reference Design Using the dsPIC® DSC"* (DS01336)

LIST OF PARAMETERS

TABLE 1: LIST OF PARAMETERS AND DESCRIPTION

Parameter	Description
V_{ref}	Reference output voltage
G_{cv}	Transfer function of voltage loop compensator
G_{delay}	Transfer functions of transportation delay
I_{ref}	Reference current
G_{ci}	Transfer function of the current loop compensator
$G_{v\omega}$	Transfer function between output voltage and switching frequency
$G_{i\omega}$	Transfer functions between inductor current and switching frequency
G_{fv}	Voltage measurement low-pass filter
G_{fc}	Current measurement low-pass filter
G_{vl}	Transfer function between output voltage and inductor current
K_p	Proportional gain of PI compensator
K_i	Integral gain of PI compensator
K_{cv}	Gain of outer voltage loop PI compensator
K_{ci}	Gain of 2P2Z compensator
i_r	Resonant inductor current
ω_s	Switching frequency
V_0	Output voltage
$K_{A/D}$	Gain of ADC measurement
TF	Transfer function

NOTES:

Note the following details of the code protection feature on Microchip devices:

- Microchip products meet the specification contained in their particular Microchip Data Sheet.
- Microchip believes that its family of products is one of the most secure families of its kind on the market today, when used in the intended manner and under normal conditions.
- There are dishonest and possibly illegal methods used to breach the code protection feature. All of these methods, to our knowledge, require using the Microchip products in a manner outside the operating specifications contained in Microchip's Data Sheets. Most likely, the person doing so is engaged in theft of intellectual property.
- Microchip is willing to work with the customer who is concerned about the integrity of their code.
- Neither Microchip nor any other semiconductor manufacturer can guarantee the security of their code. Code protection does not mean that we are guaranteeing the product as "unbreakable."

Code protection is constantly evolving. We at Microchip are committed to continuously improving the code protection features of our products. Attempts to break Microchip's code protection feature may be a violation of the Digital Millennium Copyright Act. If such acts allow unauthorized access to your software or other copyrighted work, you may have a right to sue for relief under that Act.

QUALITY MANAGEMENT SYSTEM CERTIFIED BY DNV

ISO/TS 16949

Trademarks

The Microchip name and logo, the Microchip logo, dsPIC, FlashFlex, KEELOQ, KEELOQ logo, MPLAB, PIC, PICmicro, PICSTART, PIC^{32} logo, rfPIC, SST, SST Logo, SuperFlash and UNI/O are registered trademarks of Microchip Technology Incorporated in the U.S.A. and other countries.

FilterLab, Hampshire, HI-TECH C, Linear Active Thermistor, MTP, SEEVAL and The Embedded Control Solutions Company are registered trademarks of Microchip Technology Incorporated in the U.S.A.

Silicon Storage Technology is a registered trademark of Microchip Technology Inc. in other countries.

Analog-for-the-Digital Age, Application Maestro, BodyCom, chipKIT, chipKIT logo, CodeGuard, dsPICDEM, dsPICDEM.net, dsPICworks, dsSPEAK, ECAN, ECONOMONITOR, FanSense, HI-TIDE, In-Circuit Serial Programming, ICSP, Mindi, MiWi, MPASM, MPF, MPLAB Certified logo, MPLIB, MPLINK, mTouch, Omniscient Code Generation, PICC, PICC-18, PICDEM, PICDEM.net, PICkit, PICtail, REAL ICE, rfLAB, Select Mode, SQI, Serial Quad I/O, Total Endurance, TSHARC, UniWinDriver, WiperLock, ZENA and Z-Scale are trademarks of Microchip Technology Incorporated in the U.S.A. and other countries.

SQTP is a service mark of Microchip Technology Incorporated in the U.S.A.

GestIC and ULPP are registered trademarks of Microchip Technology Germany II GmbH & Co. & KG, a subsidiary of Microchip Technology Inc., in other countries.

All other trademarks mentioned herein are property of their respective companies.

Printed on recycled paper.

ISBN: 978-1-62077-049-8

Microchip received ISO/TS-16949:2009 certification for its worldwide headquarters, design and wafer fabrication facilities in Chandler and Tempe, Arizona; Gresham, Oregon and design centers in California and India. The Company's quality system processes and procedures are for its PIC® MCUs and dsPIC® DSCs, KEELOQ® code hopping devices, Serial EEPROMs, microperipherals, nonvolatile memory and analog products. In addition, Microchip's quality system for the design and manufacture of development systems is ISO 9001:2000 certified.

Worldwide Sales and Service

AMERICAS

Corporate Office
2355 West Chandler Blvd.
Chandler, AZ 85224-6199
Tel: 480-792-7200
Fax: 480-792-7277
Technical Support:
http://www.microchip.com/support
Web Address:
www.microchip.com

Atlanta
Duluth, GA
Tel: 678-957-9614
Fax: 678-957-1455

Boston
Westborough, MA
Tel: 774-760-0087
Fax: 774-760-0088

Chicago
Itasca, IL
Tel: 630-285-0071
Fax: 630-285-0075

Cleveland
Independence, OH
Tel: 216-447-0464
Fax: 216-447-0643

Dallas
Addison, TX
Tel: 972-818-7423
Fax: 972-818-2924

Detroit
Farmington Hills, MI
Tel: 248-538-2250
Fax: 248-538-2260

Indianapolis
Noblesville, IN
Tel: 317-773-8323
Fax: 317-773-5453

Los Angeles
Mission Viejo, CA
Tel: 949-462-9523
Fax: 949-462-9608

Santa Clara
Santa Clara, CA
Tel: 408-961-6444
Fax: 408-961-6445

Toronto
Mississauga, Ontario, Canada
Tel: 905-673-0699
Fax: 905-673-6509

ASIA/PACIFIC

Asia Pacific Office
Suites 3707-14, 37th Floor
Tower 6, The Gateway
Harbour City, Kowloon
Hong Kong
Tel: 852-2401-1200
Fax: 852-2401-3431

Australia - Sydney
Tel: 61-2-9868-6733
Fax: 61-2-9868-6755

China - Beijing
Tel: 86-10-8569-7000
Fax: 86-10-8528-2104

China - Chengdu
Tel: 86-28-8665-5511
Fax: 86-28-8665-7889

China - Chongqing
Tel: 86-23-8980-9588
Fax: 86-23-8980-9500

China - Hangzhou
Tel: 86-571-2819-3187
Fax: 86-571-2819-3189

China - Hong Kong SAR
Tel: 852-2943-5100
Fax: 852-2401-3431

China - Nanjing
Tel: 86-25-8473-2460
Fax: 86-25-8473-2470

China - Qingdao
Tel: 86-532-8502-7355
Fax: 86-532-8502-7205

China - Shanghai
Tel: 86-21-5407-5533
Fax: 86-21-5407-5066

China - Shenyang
Tel: 86-24-2334-2829
Fax: 86-24-2334-2393

China - Shenzhen
Tel: 86-755-8864-2200
Fax: 86-755-8203-1760

China - Wuhan
Tel: 86-27-5980-5300
Fax: 86-27-5980-5118

China - Xian
Tel: 86-29-8833-7252
Fax: 86-29-8833-7256

China - Xiamen
Tel: 86-592-2388138
Fax: 86-592-2388130

China - Zhuhai
Tel: 86-756-3210040
Fax: 86-756-3210049

ASIA/PACIFIC

India - Bangalore
Tel: 91-80-3090-4444
Fax: 91-80-3090-4123

India - New Delhi
Tel: 91-11-4160-8631
Fax: 91-11-4160-8632

India - Pune
Tel: 91-20-2566-1512
Fax: 91-20-2566-1513

Japan - Osaka
Tel: 81-6-6152-7160
Fax: 81-6-6152-9310

Japan - Tokyo
Tel: 81-3-6880- 3770
Fax: 81-3-6880-3771

Korea - Daegu
Tel: 82-53-744-4301
Fax: 82-53-744-4302

Korea - Seoul
Tel: 82-2-554-7200
Fax: 82-2-558-5932 or
82-2-558-5934

Malaysia - Kuala Lumpur
Tel: 60-3-6201-9857
Fax: 60-3-6201-9859

Malaysia - Penang
Tel: 60-4-227-8870
Fax: 60-4-227-4068

Philippines - Manila
Tel: 63-2-634-9065
Fax: 63-2-634-9069

Singapore
Tel: 65-6334-8870
Fax: 65-6334-8850

Taiwan - Hsin Chu
Tel: 886-3-5778-366
Fax: 886-3-5770-955

Taiwan - Kaohsiung
Tel: 886-7-213-7828
Fax: 886-7-330-9305

Taiwan - Taipei
Tel: 886-2-2508-8600
Fax: 886-2-2508-0102

Thailand - Bangkok
Tel: 66-2-694-1351
Fax: 66-2-694-1350

EUROPE

Austria - Wels
Tel: 43-7242-2244-39
Fax: 43-7242-2244-393

Denmark - Copenhagen
Tel: 45-4450-2828
Fax: 45-4485-2829

France - Paris
Tel: 33-1-69-53-63-20
Fax: 33-1-69-30-90-79

Germany - Munich
Tel: 49-89-627-144-0
Fax: 49-89-627-144-44

Italy - Milan
Tel: 39-0331-742611
Fax: 39-0331-466781

Netherlands - Drunen
Tel: 31-416-690399
Fax: 31-416-690340

Spain - Madrid
Tel: 34-91-708-08-90
Fax: 34-91-708-08-91

UK - Wokingham
Tel: 44-118-921-5869
Fax: 44-118-921-5820

11/29/12